Adsorption and diffusion of gold adatoms on graphene nanoribbons: An *ab initio* study

W. H. Brito and R. H. Miwa
Instituto de Física, Universidade Federal de Uberlândia, CP 593, 38400-902 Uberlândia, MG, Brazil
(Received 10 May 2010; revised manuscript received 17 June 2010; published 20 July 2010)

We have performed a theoretical *ab initio* investigation, within the density-functional theory, of Au adatoms on graphene nanoribbons (Au/GNRs). We have considered armchair GNR (A-GNR) and zigzag GNR (Z-GNR). For both systems, we find an energetic preference for Au adatoms lying along the edge sites. Our calculated adsorption energies, 1.01 eV and 2.18 eV for Au adatoms on the A-GNR and Z-GNR, respectively, indicate the formation of Au-C covalent bonds. Au atoms can adsorb more easily along the zigzag edges than along the armchair edges. In addition, we examined the diffusion barriers of Au adatoms on those ribbon systems. We have considered a number of Au diffusion paths perpendicular as well as parallel to the ribbon growth directions. Our calculated energy barriers indicate that the segregation of Au adatoms from the inner sites toward the edge sites is a quite likely process. In this case, we find a net energy barrier of ~80 meV. In contrast, the Au adatoms will face higher energy barriers for diffusion paths along the edge sites of the ribbons. The electronic-structure calculations indicate that the semiconducting character of the GNRs has been kept for low concentration of Au adatoms. Meanwhile, by increasing the concentration of Au adatoms along the edge sites, the Au/GNR systems become metallic.

DOI: 10.1103/PhysRevB.82.045417 PACS number(s): 73.22.−f, 73.22.Pr

I. INTRODUCTION

Since the experimental realization of free-standing structures composed by a single layer of a hexagonal network of carbon atoms,[1,2] graphene has been the subject of numerous experimental and theoretical investigations. The most of those studies are focusing on future applications for a new generation of electronic devices,[3] as well as fundamental issues such as the observation of Dirac fermions in graphene.[4] In parallel, there are several groups working on new structures composed by ribbons of graphene with a width of few nanometers, graphene nanoribbons (GNRs). Indeed, recently very thin GNRs with width below 10 nm have been successfully synthesized.[5]

GNRs exhibit one-dimensional electronic confinement perpendicularly to the ribbon growth direction.[6] The electronic properties of the GNRs are strongly related to the width of the ribbons[7] and the atomic structure along the edges.[8–10] In those systems, the understanding and control of the atomic and electronic properties are quite important to build up electronic devices, such as transistors[11] and spin valves.[12,13] In general the edge sites present different reactivity when compared with the inner sites of graphene sheets. For instance, the *n*-type doping of GNRs through adsorption of NH_3 molecules along the edge sites.[14] In this case, the GNR is (covalently) functionalized by N atoms. Similar energetic preference for the edge sites is somewhat expected for other elements on GNRs. In a recent theoretical study, Power *et al.*[15] proposed an impurity segregation model on GNRs.

Metal atoms adsorbed onto graphene sheets represent a new route for the development of new electronic/spintronic devices and applications in catalysis processes. The electronic, structural, and magnetic properties of transition metals on graphene sheets[16–18] and ribbons[19–21] have been intensively studied based on *ab initio* density-functional theory (DFT). Further investigations, based upon the same theoretical approach, examined the adsorption, diffusion, and the formation of clusters of gold adatoms on graphite[22,23] and graphene sheets.[24] Gold contacts are present in several electronic devices, and thus, it is important to understand the electronic, structural, and the energetic properties of Au adatoms on graphene sheet and ribbons. In a recent experimental work, Gan *et al.*[25] obtained energy barriers of 2.5 eV for Au and Pt diffusion on graphene surface. Those results indicate the formation of Au-C and Pt-C covalent bonds, where they assume the presence of vacancies or multivacancies along the metal diffusion path. Total energy calculations considering the presence of multivacancies along the Au diffusion barriers, performed by Malola *et al.*,[26] provided further support to the experimental results. We can infer that the presence of structural defects (such as vacancies or edges in GNRs) should play an important role on the diffusion processes of adatoms on a given graphene substrate.

In the present work, we have performed an *ab initio* total-energy investigation of Au adatoms on GNRs, Au/GNRs. We have considered hydrogen-passivated armchair GNR (A-GNR) and zigzag GNR (Z-GNR) ribbon structures. Our results indicate an energetic preference of Au adatoms lying along the edge sites of the GNRs. The Au adatoms are covalently attached to the edge C atoms. We obtained binding energies of 1.01 eV and 2.18 eV for Au adatoms on A-GNR and Z-GNR, respectively. The diffusion barriers of Au adatoms on GNRs have been examined by considering a number of Au diffusion paths. We find that Au adatoms can easily segregate, at room temperature, from the inner sites toward the edge sites of the ribbons. For Au diffusion along the edge (subedge) sites of the GNRs, we find higher energy barriers, viz.: about 0.3 eV (0.1 eV) and 0.8 eV (0.4 eV) for A-GNR and Z-GNR, respectively. Finally, based upon our electronic band-structure calculations, we verify that the semiconducting character of the GNRs has been maintained, for low concentration of Au adatoms. In contrast, by increasing the Au coverage, the Au/GNR system becomes metallic.

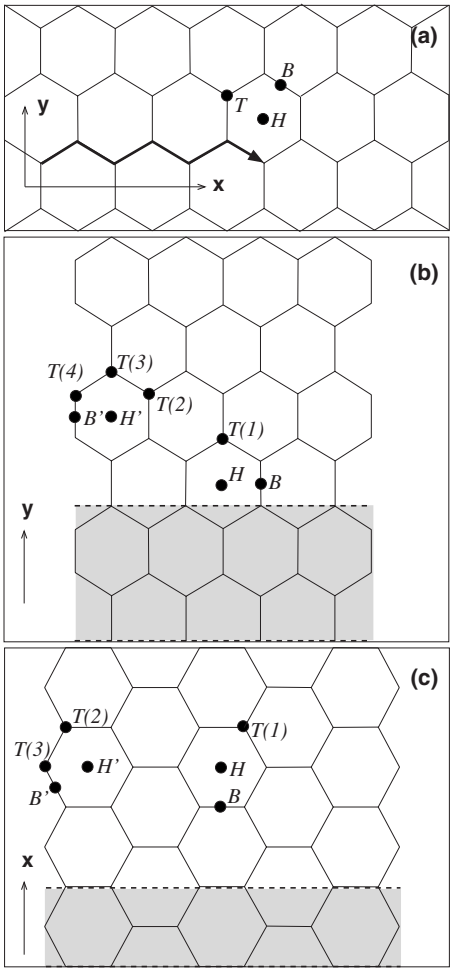

FIG. 1. Adsorption sites on the (a) graphene sheet, (b) (3×5) A-GNR, and (c) (4×6) Z-GNR. The arrow in (a) indicates the lowest energy Au diffusion path. Shaded region represents the periodic unit of the supercells. The hydrogen atoms are not shown.

II. METHOD OF CALCULATION

The calculations were performed based upon the density-functional theory within the local spin-density approximation.[27,28] The Au/A-GNR and Au/Z-GNR systems were described by using the supercells approach, as depicted in Figs. 1(b) and 1(c), respectively. The supercell of A-GNR exhibits a (3×5) surface periodicity with 54 C atoms/supercell. Namely, it is composed by three periodic units, indicated by the shaded region in Fig. 1(b), along the ribbon growth direction and a width of five consecutive C-C bonds. While the supercell of Z-GNR presents a (4×6) surface periodicity with 48 C atoms/supercell. That is, four periodic units [shaded region in Fig. 1(c)] piled up along the ribbon growth direction and a width of six consecutive C-C bonds. The edge C dangling bonds are saturate with hydrogen atoms. In order to avoid the interaction between the Au/GNR and its image, due to the periodic boundary conditions, vacuum regions of ~11 Å (15 Å) perpendicular (parallel) to the GNRs have been included. The self-consistent total charge density was obtained by using a set of 6 (16) special **k** points to sample the respective Brillouin zone of A-GNR (Z-GNR). All the atomic positions were relaxed by using the conjugated gradient scheme, within a force convergence criterion of 10 meV/Å.

The Au adsorption energies, equilibrium geometries, and the electronic structure were calculated by using the SIESTA code.[29] The Kohn-Sham orbitals were described by linear combinations of numerical pseudoatomic orbitals using a split-valence double-zeta basis set including polarization functions. We have considered an energy shift of 0.10 eV (Ref. 29) to determine the cutoff radius of the pseudoatomic orbitals. The electron-ion interactions were calculated using norm-conserving pseudopotentials.[30] The calculation of the Au diffusion paths were performed by using the climbing-image nudged-elastic band (CI-NEB) approach[31] as implemented in the PWSCF code.[32] In PWSCF the Kohn-Sham orbitals were expanded in a plane-wave basis set with energy cutoff of 30 Ry expanded to 120 Ry for the calculation of the self-consistent total charge density. Here the electron-ion interactions were described through ultrasoft pseudopotentials.[33]

The adsorption energy (E^{ads}) was calculated by comparing the total energies of the (final) Au/GNR system (E[Au/GNRs]) and the sum of the total energies of the isolated systems, GNR (E[GNR]) and Au adatom (E[Au]). E^{ads} can be written as

$$E^{ads} = E[\mathrm{Au}] + E[\mathrm{GNR}] - E[\mathrm{Au/GNRs}] - \delta^{\mathrm{BSSE}}.$$

Positive values of E^{ads} indicate that the Au adsorption onto GNR is an exothermic process. The last term, δ^{BSSE}, has been included to correct the basis-set superposition errors (BSSEs).[34] δ^{BSSE} was calculated by using the procedure proposed by Hobbs *et al.*[35]

III. RESULTS AND DISCUSSIONS

Initially we examined the adsorption energies, the equilibrium geometry, and the diffusion barrier of a single Au adatom adsorbed on graphene sheet. We considered the following plausible Au adsorption sites, viz.: on top (T), bridge (B), and hollow (H), as depicted in Fig. 1(a). Au adatoms adsorbed on the T site, $E^{ads}=0.63$ eV, represent the energetically most favorable configuration. Comparing the adsorption energies, we find that E^{ads} is slightly lower for Au adatom lying on the B site, while on the H site we obtained $E^{ads}=0.41$ eV. It is worth to point out that Au adatoms on the H sites are energetically unstable. In this case, E^{ads} on the H site was obtained by constraining the relaxation of Au adatoms (on the H site) along the z coordinate while the C atoms of the graphene sheet are free to relax in all directions. At the equilibrium geometry, for Au on the T site, the Au-C bond length is 2.22 Å, where the C atoms moves upward by 0.12 Å. Upon such vertical displacement we find a strain energy of 0.13 eV on the graphene sheet.[36] Those results are in good agreement with previous *ab initio* DFT calculations performed within the same local-density approximation.[22,24] Finally, within the CI-NEB approach (considering 20 images), we calculate the diffusion barrier of Au adatoms on graphene. As expected from our calculated adsorption energies, the H site does not belong to the lowest energy diffu-

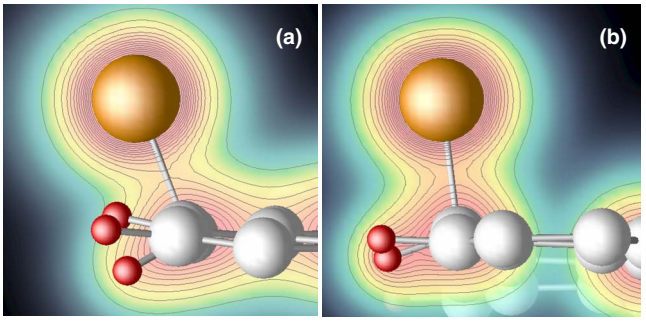

FIG. 2. (Color online) Total charge density along the Au-C bonds of (a) $Au^{(T4)}$/A-GNR and (b) $Au^{(T3)}$/Z-GNR.

sion path for Au adatoms. We find an energy barrier (E^b) of 0.028 eV where the Au atoms follow $T \rightarrow B \rightarrow T$ configurations [indicated by an arrow in Fig. 1(a)]. Jensen *et al.*,[31] based upon NEB approach obtained similar diffusion path and a slightly higher energy barrier, 0.05 ± 0.01 eV.

Au adatoms present quite different energetic, structural, and electronic properties nearby the edge sites of GNRs. The edge states of GNRs exhibit a high density of states (composed by π and π^* orbitals) near the Fermi level, and thus, it is expected an energetic preference for Au adsorption at the edge sites. The Au adsorption sites are indicated in Figs. 1(b) and 1(c) for the Au/A-GNR and Au/Z-GNR, respectively. Here all the atomic coordinates of the GNRs and the Au adatoms are free to relax. After structural optimizations, we find that the Au adatoms are energetically unstable on the hollow and bridge sites around the edges of GNRs, H' and B' sites, respectively, in Figs. 1(b) and 1(c). Au adatoms placed on those sites migrate to the nearly T site. Comparing the calculated total energies we verify that there is an energetic preference for the T sites on top of the edge C atoms, viz., $T(4)$ for Au adatoms on the A-GNR ($Au^{T(4)}$/A-GNR) and $T(3)$ for Au adatoms on the Z-GNR ($Au^{T(3)}$/Z-GNR). In addition, on Z-GNR we verify that Au adatoms on the subedge site, $T(2)$, is not an energetically stable configuration. At the equilibrium geometry the Au-C bond lengths are 2.10 ($Au^{T(4)}$/A-GNR) and 2.03 Å ($Au^{T(3)}$/Z-GNR), being 0.12 Å and 0.19 Å, respectively, smaller than Au-C bond length on the graphene sheet. The C atom (underneath the Au adatom) moves upward by 0.05 Å and 0.37 Å for the A-GNR and Z-GNR, respectively, and the induced strain energies are 0.32 eV ($Au^{T(4)}$/A-GNR) and 0.67 eV ($Au^{T(3)}$/Z-GNR).[36] Those strain energies are larger when compared with the one on the graphene sheet, however, they are compensated by the formation of stable Au-C covalent bonds. Figures 2(a) and 2(b) present the total change density along the Au-C bonds for $Au^{T(4)}$/A-GNR and $Au^{T(3)}$/Z-GNR, respectively. Our calculated adsorption energies, summarized in Table I, reveal that Au adatoms are more strongly bonded on the GNRs, when compared with Au adatom on the graphene sheets, being Au adatoms along the edge sites, $Au^{T(4)}$/A-GNR and $Au^{T(3)}$/Z-GNR, the most likely configurations. Indeed, the energetic preference for the edge sites is in accordance with recently proposed atomic segregation model in GNRs.[15] Furthermore, our total-energy results indicate that the Au adatoms are more tightly bonded on the zigzag edges in comparison with the ones on the armchair edges. Thus, we can infer that in disordered edges, where we have a mixture of armchair and zigzag geometries, the Au adatoms will concentrate (mostly) at the zigzag edges. On the other hand, kinetic factors will play an important rule on the atomic distribution of Au adatoms on a given surface.

TABLE I. Adsorption energies, E^{ads} (in eV/atom), of Au adatom on A-GNR and Z-GNR.

Au/GNR	$T(1)$	$T(2)$	$T(3)$	$T(4)$
A-GNR	0.68	0.73	0.68	1.01
Z-GNR	0.86	Unstable	2.18	

In order to get a more complete picture of Au/GNRs, we examine the Au diffusion on the A-GNR and Z-GNR. The calculations of the energy barriers were performed based upon CI-NEB approach.[31] Figure 3(a) presents the considered diffusion paths for an Au adatom on Au/A-GNR. Figures 3(b)–3(d) present the calculated energy barriers as a function of the Au diffusion coordinate q (q represents the Au coordinate along the minimum energy diffusion path). Here we set $q=0$ for the initial (x_0, y_0, z_0) position and $q=1$ for the final (x_1, y_1, z_1) position of the Au adatom. During the Au diffusion process from the central $T(1)$ site to the edge $T(4)$ site, the adatom goes through $T \rightarrow B \rightarrow T$ sites, path 1 in Fig. 3(a). The diffusion path does not pass through the hollow site, similar to the diffusion path obtained for Au adatom on graphene sheet. We notice that around the central region of A-GNR the diffusion barrier from $T^{(1)}$ to the nearest-neighbor T site is 0.045 eV, which is slightly larger than the energy barrier for an Au adatoms on the graphene sheet (0.028 eV). The Au adatom will face a higher energy barrier, 0.080 eV, at $q=0.37$. Whereas for $q>0.37$ the Au adatom moves to $T(4)$ almost with no energy barrier, Fig. 3(b). Those results indicate that Au adatoms can easily segregate, at room temperature, toward the edge sites of A-GNRs. In contrast, we find higher energy barriers for Au adatoms moving along the edge sites. Here we have considered two different diffusion paths, namely, 2 and 3 in Fig. 3(a), where we find energy barriers of 0.42 eV and 0.33 eV, respectively, Fig. 3(c). In the path 2 the Au adatom moves from one $T(4)$ site to another (equivalent) $T(4)$ site passing through an edge H site, $T(4) \rightarrow H \rightarrow T(4)$. The energy barrier is 0.42 eV on the H site. For the diffusion path 3, we have imposed additional constraints to the Au atomic displacements within the CI-NEB approach. In this case, we find energy barriers of 0.28 eV for $T(4) \leftrightarrow T(3)$, and 0.05 eV for $T(3) \rightarrow B \rightarrow T(3)$. Finally, along the subedge sites [path 4 in Fig. 3(a)], the Au adatom follows the $T(3) \rightarrow T(2) \rightarrow T(2) \rightarrow T(3)$ diffusion path, passing through the B sites. We find an energy barrier for $T(2) \rightarrow T(2)$, 0.05 eV, while for $T(2) \rightarrow T(3)$ the Au adatom will face an energy barrier of 0.11 eV, Fig. 3(d). The energy barriers for Au adatoms moving along the subedge sites are lower compared with the ones obtained for the edge sites.

We next examine the Au diffusion on Z-GNR. The Au diffusion paths are depicted in Fig. 4(a). The calculated en-

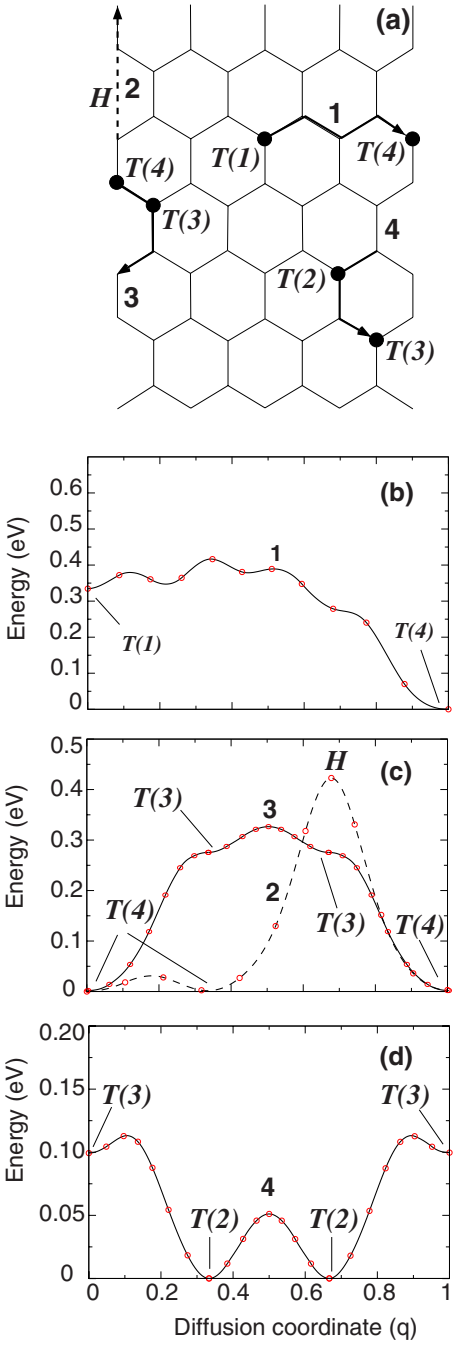

FIG. 3. (Color online) Diffusion paths of Au adatoms on A-GNR (a), and the calculated energy barriers, from the inner sites toward the edge sites (b), along the edge sites (c), and along the subedge sites (d).

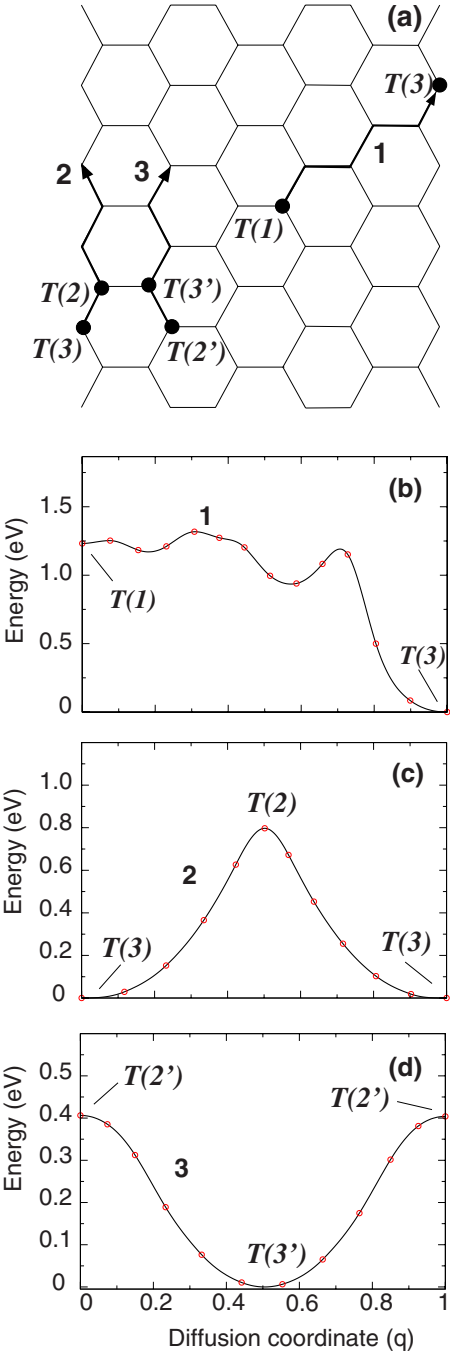

FIG. 4. (Color online) Diffusion paths of Au adatoms on Z-GNR (a), and the calculated energy barriers, from the inner sites toward the edge sites (b), along the edge sites (c), and along the subedge sites (d).

ergy barrier along the path 1 [Fig. 4(b)] indicates that the Au adatom follows the $T \rightarrow B \rightarrow T$ sites with a net energy barrier of 0.085 eV at $q=0.3$. There is a local minimum (maximum) at $q=0.58$ [nearby $T(2)$, $q=0.7$] before the Au adatom reaches to the edge $T(3)$ site. Figures 4(c) and 4(d) present the energy barrier for Au adatoms along the edge and subedge sites, respectively. Along the edge sites the Au adatom follows the $T(3) \rightarrow T(2) \rightarrow T(3)$ diffusion path. There is an energy barrier of 0.80 eV around the $T(2)$ site ($q=0.5$). While along the subedge sites, path 3, the energy barrier reduces to 0.40 eV, Fig. 4(d). In this case, the Au adatom passes through $T(2') \rightarrow T(3') \rightarrow T(2')$ sites. In summary, for both systems (Au/A-GNR and Au/Z-GNR) we can infer that the Au adatoms can easily segregate toward the edge sites at room temperature. In contrast, Au diffusion along or nearby the edge sites will be more difficult, where zigzag edges present higher energy barriers in comparison with the ones on the armchair edges.

For the energetically most stable $Au^{T(4)}$/A-GNR and $Au^{T(3)}$/Z-GNR structures, we observe strong electronic inter-

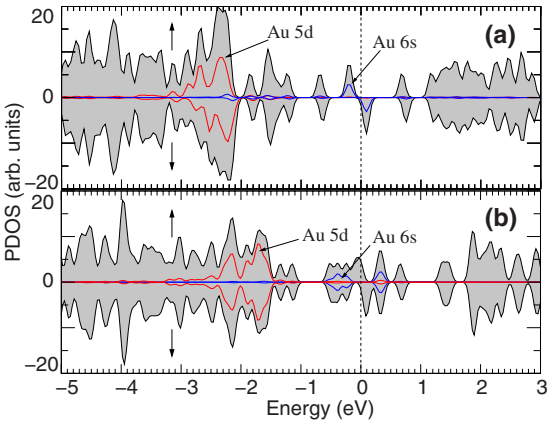

FIG. 5. (Color online) Density of states of (a) $Au^{T(4)}$/A-GNR and (b) $Au^{T(3)}$/Z-GNR. Shaded regions indicate the total density of states and the solid lines indicate the projected density of states. Spin-up and spin-down contributions are presented along the positive and negative y axes, respectively. Along the horizontal axis, the zero corresponds to the Fermi level.

actions between the electronic states of Au ($5d$ and $6s$) and the neighboring C $2p_z$, as indicated in Fig. 5. We find that the Au $5d$ orbitals spread out within an energy interval between 1.5 and 3.0 eV below the Fermi level (E_F), whereas the Au $6s$ states lie at around $E_F \pm 0.8$ eV. On the Au/A-GNR the Au $6s$ states orbital become spin polarized. The semiconducting character of A-GNR and the Z-GNR has been maintained. Figures 6(a) and 6(c) present the electronic band structures of pristine A-GNR and Z-GNR, respectively. For $Au^{T(4)}$/A-GNR, Fig. 6(b), we find a very localized occupied spin-up (empty spin-down) electronic state lying at ~0.4 eV (~0.6 eV) above the valence-band maximum. Those states are mostly composed by Au $6s$ and the C $2p_z$ as indicated in Fig. 5(a). In contrast, as indicated in Fig. 5(b), there are no Au contribution to the highest-occupied spin-up ($v1$) and the lowest-unoccupied spin-down ($c1$) states in the $Au^{T(3)}$/Z-GNR, Fig. 6(d). $v1$ comes from the C $2p_z$ orbitals localized along the zigzag edge opposite to the Au adsorption site while $c1$ lies at the same edge where the Au adatoms are adsorbed.

Since the Au segregation toward the edge sites of the ribbons is quite likely, we next calculate the electronic band structure of Au/A-GNR and Au/Z-GNR for higher concentrations of Au adatoms along the GNR edges. We have considered two plausible geometries as depicted in Figs. 7(a) and 7(b). Here we have considered (2×5) and (2×6) supercells to describe the Au/A-GNR and Au/Z-GNR, respectively. Upon Au adsorption on Z-GNR, its magnetic moment is suppressed along the Au adsorbed (edge) sites. The electronic band structure of the pristine systems are shown in Figs. 6(e) and 6(g). Meanwhile, our electronic band-structure calculations indicate that both systems, Au/A-GNR [Fig. 6(f)] and Au/Z-GNR [Fig. 6(h)] become metallic by increasing the concentration of Au adatoms. The partially occupied states are localized along the Au chains and the neighboring C atoms of the ribbons. In those systems, the lateral distance between the Au adatom are 4.30 Å (Au/A-GNR) and 2.50 Å (Au/Z-GNR), and thus, we verify an electronic overlap between nearest-neighbor Au adatoms as depicted in Fig. 7. In the same diagram we present the electronic distribution of the partially occupied states within an energy range of $E_F \pm 0.20$ eV. Those results suggest that we may have metallic channels along Au chains adsorbed onto GNRs.

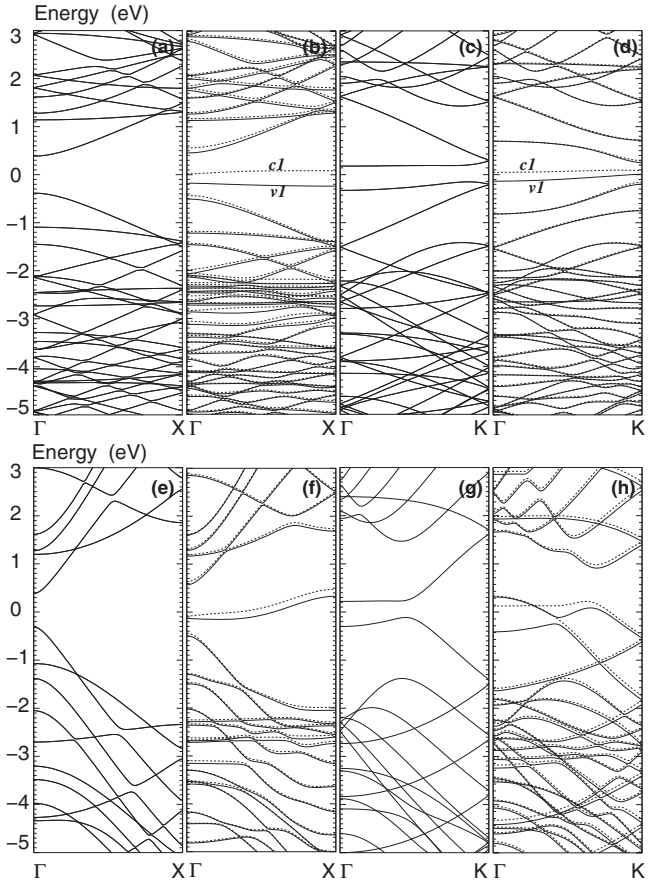

FIG. 6. Electronic band structures of Au/GNRs for low concentration of Au adatoms. (a) Pristine (3×5) A-GNR, (b) $Au^{T(4)}$/A-GNR, (c) pristine (4×6) Z-GNR, and (d) $Au^{T(3)}$/Z-GNR. Electronic band structures for higher concentration of Au adatoms, (e) pristine (2×5) A-GNR, (f) $Au^{T(4)}$/A-GNR, (g) pristine (2×6) Z-GNR, and (h) $Au^{T(3)}$/Z-GNR. Solid (dashed) lines indicate the spin-up (spin-down) components.

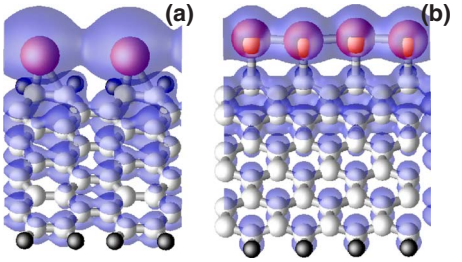

FIG. 7. (Color online) Structural models and the charge densities of the partially occupied states (within an energy interval of $E_F \pm 0.2$ eV) for higher concentration of Au adatoms on (a) Au/A-GNR and (b) Au/Z-GNR. The isosurfaces correspond to charge densities of $5\times10^{-4} e/\text{bohr}^3$.

IV. SUMMARY

We have performed an *ab initio* total-energy investigation of Au adatoms on the GNRs. We find that the Au adsorption energies are higher on the edge sites, in comparison with E^{ads} on the graphene sheet. We have considered A-GNR and Z-GNR, where we obtained an energetic preference for Au adatoms lying on the zigzag edges. Those findings allow us to infer that along the disordered edges, i.e., a mixture of armchair and zigzag geometries, the Au adatoms will concentrate (mostly) on the zigzag edges. Further Au diffusion barrier calculations indicate that for both systems, Au/A-GNR and Au/Z-GNR, the Au adatoms can easily segregate (at room temperature) from the inner sites toward the edge sites of the ribbons. In contrast, Au diffusion parallel to the ribbon growth direction (along the edges) will be more difficult. In this case, Au adatoms will face higher energy barriers, between 0.4–0.8 eV along the edge sites. While, along the subedge sites energy barriers become lower, 0.1–0.4 eV. The energy barrier for Au diffusion along the GNRs reduces as a function of the lateral distance from the edge sites. For lower concentration of Au adatoms along the edge sites, we find that the semiconducting character of the GNRs has been maintained. Whereas, increasing the concentrations of Au adatoms, our electronic band-structure calculations reveal that Au/GNRs become metallic, giving rise to metallic channels composed of Au adatoms along the ribbons.

ACKNOWLEDGMENTS

The authors acknowledge G. P. Srivastava for his comments and suggestions on the manuscript. This work received the financial support from the Brazilian agencies CNPq, CAPES, and FAPEMIG, and computational support from CENAPAD/SP.

[1] K. S. Novoselov, A. K. Geim, S. V. Morozov, D. Jiang, Y. Zhang, S. V. Dubonos, V. Grigoreva, and A. A. Firsov, Science **306**, 666 (2004).
[2] K. S. Novoselov, D. Jiang, F. Shedin, T. J. Booth, V. V. Khotkevich, S. V. Morozov, and A. K. Geim, Proc. Natl. Acad. Sci. U.S.A. **102**, 10451 (2005).
[3] S. Stankovich, D. A. Dikin, G. H. B. Dommett, K. M. Kohlhaas, E. J. Zimney, E. A. Stach, R. D. Piner, S. T. Nguyen, and R. S. Ruoff, Nature (London) **442**, 282 (2006).
[4] S. Y. Zhou, G. H. Gweon, J. Graf, A. V. Fedorov, C. D. Spataru, D. H. Diehl, Y. Kopelevich, D. H. Lee, S. G. Louie, and A. Lanzara, Nat. Phys. **2**, 595 (2006).
[5] X. Li, X. Wang, L. Zhang, S. Lee, and H. Dai, Science **319**, 1229 (2008).
[6] L. G. Cançado, M. A. Pimenta, B. R. A. Neves, G. Medeiros-Ribeiro, T. Enoki, Y. Kobayashi, K. Takai, K. Fukui, M. S. Dresselhaus, R. Saito, and A. Jorio, Phys. Rev. Lett. **93**, 047403 (2004).
[7] Y.-W. Son, M. L. Cohen, and S. G. Louie, Phys. Rev. Lett. **97**, 216803 (2006).
[8] H. Lee, Y.-W. Son, N. Park, S. Han, and J. Yu, Phys. Rev. B **72**, 174431 (2005).
[9] E. R. Mucciolo, A. H. Castro Neto, and C. H. Lewenkopf, Phys. Rev. B **79**, 075407 (2009).
[10] K. A. Ritter and J. W. Lyding, Nature Mater. **8**, 235 (2009).
[11] X. Wang, Y. Ouyang, X. Li, H. Wang, J. Guo, and H. Dai, Phys. Rev. Lett. **100**, 206803 (2008).
[12] Y.-W. Son, M. L. Cohen, and S. G. Louie, Nature (London) **444**, 347 (2006).
[13] T. B. Martins, R. H. Miwa, A. J. R. da Silva, and A. Fazzio, Phys. Rev. Lett. **98**, 196803 (2007).
[14] X. Wang, X. Li, L. Zhang, Y. Yoon, P. K. Weber, H. Wang, J. Guo, and H. Dai, Science **324**, 768 (2009).
[15] S. R. Power, V. M. de Menezes, S. B. Fagan, and M. S. Ferreira, Phys. Rev. B **80**, 235424 (2009).
[16] K. T. Chan, J. B. Neaton, and M. L. Cohen, Phys. Rev. B **77**, 235430 (2008).
[17] A. V. Krasheninnikov, P. O. Lehtinen, A. S. Foster, P. Pyykkö, and R. M. Nieminen, Phys. Rev. Lett. **102**, 126807 (2009).
[18] D. W. Boukhvalov and M. I. Katsnelson, Appl. Phys. Lett. **95**, 023109 (2009).
[19] E. J. Kan, H. J. Xiang, J. Yang, and J. G. Hou, J. Chem. Phys. **127**, 164706 (2007).
[20] H. Sevinçli, M. Topsakal, E. Durgun, and S. Ciraci, Phys. Rev. B **77**, 195434 (2008).
[21] V. A. Rigo, T. B. Martins, A. J. R. da Silva, A. Fazzio, and R. H. Miwa, Phys. Rev. B **79**, 075435 (2009).
[22] P. Jensen, X. Blase, and P. Ordejón, Surf. Sci. **564**, 173 (2004).
[23] J. Akola and H. Häkkinen, Phys. Rev. B **74**, 165404 (2006).
[24] R. Varns and P. Strange, J. Phys.: Condens. Matter **20**, 225005 (2008).
[25] Y. Gan, L. Sun, and F. Banhart, Small **4**, 587 (2008).
[26] S. Malola, H. Häkkinen, and P. Koskinen, Appl. Phys. Lett. **94**, 043106 (2009).
[27] D. M. Ceperley and B. J. Alder, Phys. Rev. Lett. **45**, 566 (1980).
[28] J. P. Perdew and A. Zunger, Phys. Rev. B **23**, 5048 (1981).
[29] J. M. Soler, E. Artacho, J. D. Gale, A. García, J. Junquera, P. Ordejón, and D. Sánchez-Portal, J. Phys.: Condens. Matter **14**, 2745 (2002).
[30] N. Troullier and J. L. Martins, Phys. Rev. B **43**, 1993 (1991).
[31] G. Henkelman, B. P. Uberuaga, and H. Jónsson, J. Chem. Phys. **113**, 9901 (2000).
[32] P. Giannozzi, S. Baroni, N. Bonini, M. Calandra, R. Car, C. Cavazzoni, D. Ceresoli, G. L. Chiarotti, M. Cococcioni, I. Dabo, A. Dal Corso, S. de Gironcoli, S. Fabris, G. Fratesi, R. Gebauer, U. Gerstmann, C. Gougoussis, A. Kokalj, M. Lazzeri, L. Martin-Samos, N. Marzari, F. Mauri, R. Mazzarello, S. Paolini, A. Pasquarello, L. Paulatto, C. Sbraccia, S. Scandolo, G. Sclauzero, A. P. Seitsonen, A. Smogunov, P. Umari, and R. M. Wentzcovitch, J. Phys.: Condens. Matter **21**, 395502 (2009).
[33] D. Vanderbilt, Phys. Rev. B **41**, 7892 (1990).
[34] S. F. Boys and F. Bernardi, Mol. Phys. **19**, 553 (1970).
[35] C. Hobbs, K. Kantorovich, and J. D. Gale, Surf. Sci. **591**, 45 (2005).

[36] The surface strain energy (E^s) is defined as, $E^s = E^{strain} - E^{relax}$. The latter represents the total energy of the relaxed system, pristine GNR, and E^{strain} represents the total energy of the strained system. This term was calculated keeping the C atoms at the equilibrium geometry as that obtained for the Au adsorbed system. The adsorbate (Au adatom) should be excluded in E^{strain}.